Cell Reports

Neuronal Mitochondrial Dysfunction Activates the Integrated Stress Response to Induce Fibroblast Growth Factor 21

Graphical Abstract

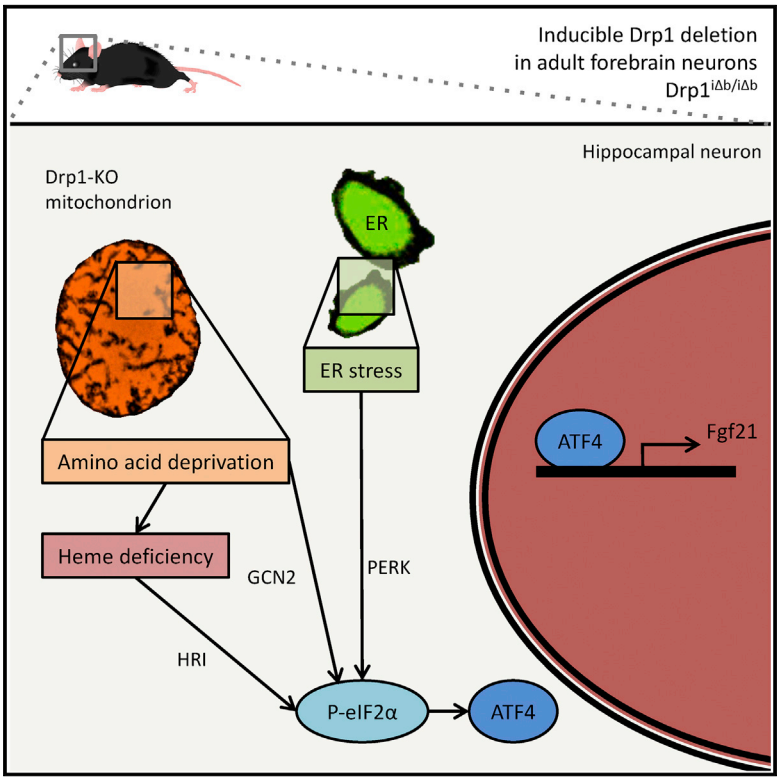

Highlights

- Neuronal Drp1 ablation is sensed by branches of the integrated stress response (ISR)
- Activation of the ISR induces catabolic cytokine Fgf21 in the brain
- Brain Fgf21 induced in neurodegeneration models may be a potential biomarker

Authors

Lisa Michelle Restelli, Björn Oettinghaus, Mark Halliday, ..., Giovanna Mallucci, Luca Scorrano, Stephan Frank

Correspondence

stephan.frank@usb.ch

In Brief

Restelli et al. show that deletion of mitochondrial fission protein Drp1 in adult mouse neurons activates multiple stress-sensing pathways. These converge on the integrated stress response, resulting in neuron-specific expression of metabolic cytokine Fgf21. Cerebral induction of Fgf21 also occurs in mechanistically independent mouse models of protein misfolding-associated neurodegeneration.

Restelli et al., 2018, Cell Reports *24*, 1407–1414
August 7, 2018
https://doi.org/10.1016/j.celrep.2018.07.023

CellPress

Cell Reports
Report

Neuronal Mitochondrial Dysfunction Activates the Integrated Stress Response to Induce Fibroblast Growth Factor 21

Lisa Michelle Restelli,[1,2,11] Björn Oettinghaus,[1,11] Mark Halliday,[3] Cavit Agca,[4] Maria Licci,[5] Lara Sironi,[1,2] Claudia Savoia,[6] Jürgen Hench,[1] Markus Tolnay,[1] Albert Neutzner,[4] Alexander Schmidt,[7] Anne Eckert,[8] Giovanna Mallucci,[3,9,12] Luca Scorrano,[6,10,12] and Stephan Frank[1,12,13,*]

[1]Division of Neuropathology, Institute of Medical Genetics and Pathology, University Hospital Basel, Basel 4031, Switzerland
[2]University of Basel, Basel 4001, Switzerland
[3]Department of Clinical Neurosciences, University of Cambridge, Cambridge Biomedical Campus, Cambridge CB2 0AH, UK
[4]Departments of Biomedicine and Ophthalmology, University Hospital Basel, Basel 4031, Switzerland
[5]Department of Neurosurgery, University Hospital Basel, Basel 4031, Switzerland
[6]Department of Biology, University of Padua, Padua 35121, Italy
[7]Proteomics Core Facility, Biozentrum, University of Basel, Basel 4056, Switzerland
[8]University Psychiatric Clinics, Basel 4025, Switzerland
[9]UK Dementia Research Institute at the University of Cambridge, Cambridge Biomedical Campus, Cambridge CB2 0AH, UK
[10]Venetian Institute of Molecular Medicine, Padua 35129, Italy
[11]These authors contributed equally
[12]Senior author
[13]Lead Contact
*Correspondence: stephan.frank@usb.ch
https://doi.org/10.1016/j.celrep.2018.07.023

SUMMARY

Stress adaptation is essential for neuronal health. While the fundamental role of mitochondria in neuronal development has been demonstrated, it is still not clear how adult neurons respond to alterations in mitochondrial function and how neurons sense, signal, and respond to dysfunction of mitochondria and their interacting organelles. Here, we show that neuron-specific, inducible *in vivo* ablation of the mitochondrial fission protein Drp1 causes ER stress, resulting in activation of the integrated stress response to culminate in neuronal expression of the cytokine Fgf21. Neuron-derived Fgf21 induction occurs also in murine models of tauopathy and prion disease, highlighting the potential of this cytokine as an early biomarker for latent neurodegenerative conditions.

INTRODUCTION

In neurons, mitochondrial fission, which in mammals depends mainly on dynamin-related protein Drp1, facilitates both axonal mitochondrial transport and mitophagic elimination (Oettinghaus et al., 2016; Pernas and Scorrano, 2016; Twig et al., 2008; Wai and Langer, 2016). Not surprisingly, Drp1 is therefore required for brain development and mature neuronal function (Berthet et al., 2014; Ishihara et al., 2009; Kageyama et al., 2012; Oettinghaus et al., 2016; Shields et al., 2015; Wakabayashi et al., 2009). In several clinically and pathologically distinct neurodegenerative diseases, mitochondrial morphology is disrupted (reviewed by DuBoff et al., 2013), substantiating the link among mitochondrial dynamics, function, and brain pathophysiology. Given this, brain mitochondrial dysfunction could represent an important marker to identify subjects at risk of developing neurodegenerative disorders, before neurological symptoms manifest; however, no surrogate marker of brain mitochondrial dysfunction is available.

Mitochondria of peripheral organs (e.g., liver and muscle) can convey disruption of their function by mounting cell-wide stress responses (Cornu et al., 2014; Guridi et al., 2015; Hagiwara et al., 2012; Keipert et al., 2014; Kim et al., 2013a; Touvier et al., 2015; Tyynismaa et al., 2010). A common trait of these models is the expression, causally linked to mitochondrial dysfunction, of the metabolic cytokine fibroblast growth factor 21 (Fgf21). This cytokine exerts a plethora of tissue-specific effects and is subject to complex pharmacology and pharmacokinetics, aspects of which continue to be matter of debate (reviewed by Kharitonenkov and DiMarchi, 2017). In addition to being canonically produced by liver and white adipose tissue (WAT) in response to starvation, Fgf21 can be secreted by other organs, such as pancreas and brown adipose tissue (Degirolamo et al., 2016; Fisher and Maratos-Flier, 2016). Moreover, Fgf21 has been established as a marker of mitochondrial myopathies (Suomalainen et al., 2011; Tezze et al., 2017). Whether Fgf21 is also produced by the CNS in response to mitochondrial dysfunction is unknown. Here we capitalize on our previously generated mouse model of inducible mitochondrial fission ablation in mature forebrain neurons (Oettinghaus et al., 2016), as well as on bona fide mouse models of neurodegeneration, to demonstrate that various forms of neuronal cell stress, including mitochondrial dysfunction, are sensed by the integrated stress response (ISR). In each of these models, ISR activation leads to

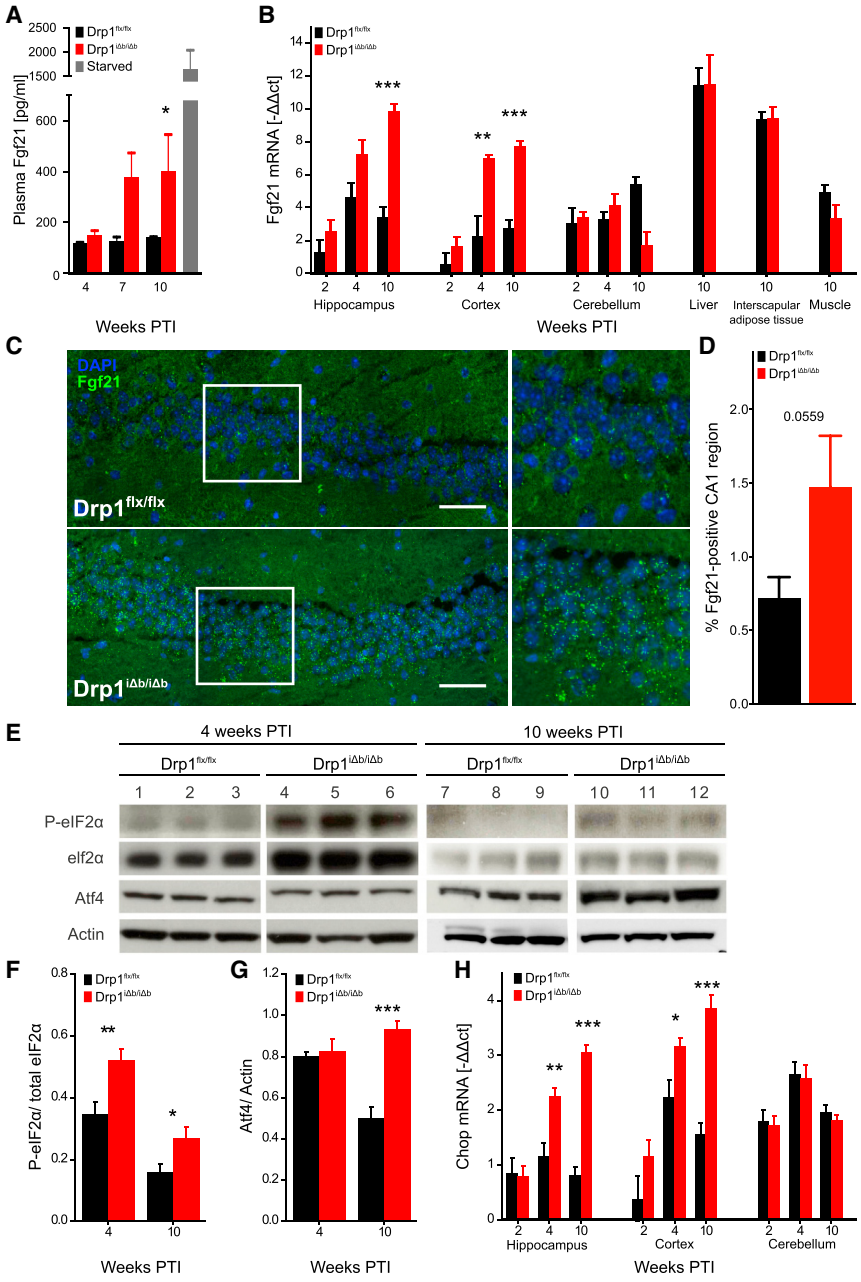

Figure 1. Neuronal *Drp1* Ablation Induces ISR-Driven Brain Fgf21 Expression

(A) FGF21 plasma levels in cardiac blood of *Drp1*-ablated and control mice. Positive control represents overnight-starved animals. Data represent average + SEM of at least 3 animals.

(B) qRT-PCR analysis of different mouse tissues at indicated time points PTI. *Fgf21* mRNA ct values normalized against 18S rRNA ct values. Data represent average + SEM of at least 4 animals.

(C and D) Representative *Fgf21* mRNA-fluorescence *in situ* hybridization (FISH) analysis of the hippocampal CA1 region of a *Drp1*-ablated mouse at 10 weeks PTI (C). Fgf21 mRNA hybridization signals are in green; nuclei are DAPI stained. Scale bar, 20 μm. Quantification of hybridization signals (D).

(E) Representative western blots of *Drp1*-ablated and control hippocampal lysates separated by SDS-PAGE and immunoblotted using indicated antibodies.

(F and G) Quantification of phosphorylated eIF2α band intensity normalized to total eIF2α (F) and Atf4 intensity normalized to actin (G). Data represent average + SEM of at least 4 animals.

(H) qRT-PCR analysis of *Chop* expression in various mouse brain regions. Data represent average + SEM of at least 4 animals.

neuron-specific Fgf21 expression, highlighting the potential of this cytokine as biomarker for neurodegenerative conditions.

RESULTS

Neuronal *Drp1* Ablation Activates the ISR, Resulting in Fgf21 Induction

We previously generated a model of inducible ablation of the mitochondrial fission protein Drp1 in the adult mouse forebrain (*Drp1*$^{flx/flx}$; *CaMKIIα::CreERT2*, tamoxifen-inducible *Drp1* deletion from brain, *Drp1*$^{iΔb/iΔb}$). In this model, neuronal *Drp1* ablation compromised mitochondrial respiration and shifted cellular metabolism toward glycolysis (Oettinghaus et al., 2016); in addition, systemic catabolic changes occurred, which prompted further investigation.

Because mitochondrial dysfunction in several peripheral organs can lead to the induction of the cytokine Fgf21 (Kharitonenkov and DiMarchi, 2015; Kim et al., 2013a; Suomalainen et al., 2011), we checked whether the same was true for a brain-specific mitochondrial defect. Starting 7 weeks post-tamoxifen injection (PTI, i.e., after *Drp1* ablation), we found elevated Fgf21 plasma levels (Figure 1A), prompting us to investigate its source organ or organs. Subsequent analyses revealed that as early as 4 weeks after *Drp1* ablation, *Fgf21* transcription was induced specifically in hippocampus and cortex but not in: the cerebellum (where the *Cre*-driving *CaMKIIα* promoter is inactive); the canonical Fgf21 sources (liver and adipose tissue); or the skeletal muscle (Figure 1B). These results establish brain as the Fgf21 tissue source in our model. mRNA fluorescence *in situ* hybridization identified neurons as the primary Fgf21 producers in the *Drp1*-ablated mouse brain, shown in Figures 1C and 1D for the hippocampal CA1 region (Figures S1A–S1C detail the histological distribution of hippocampal pyramidal neurons for reference; for comparison, Figures S1D and S1E show the distribution of astrocytes and microglia). These observations are significant from two perspectives: we demonstrate that Fgf21 can be produced by neurons in

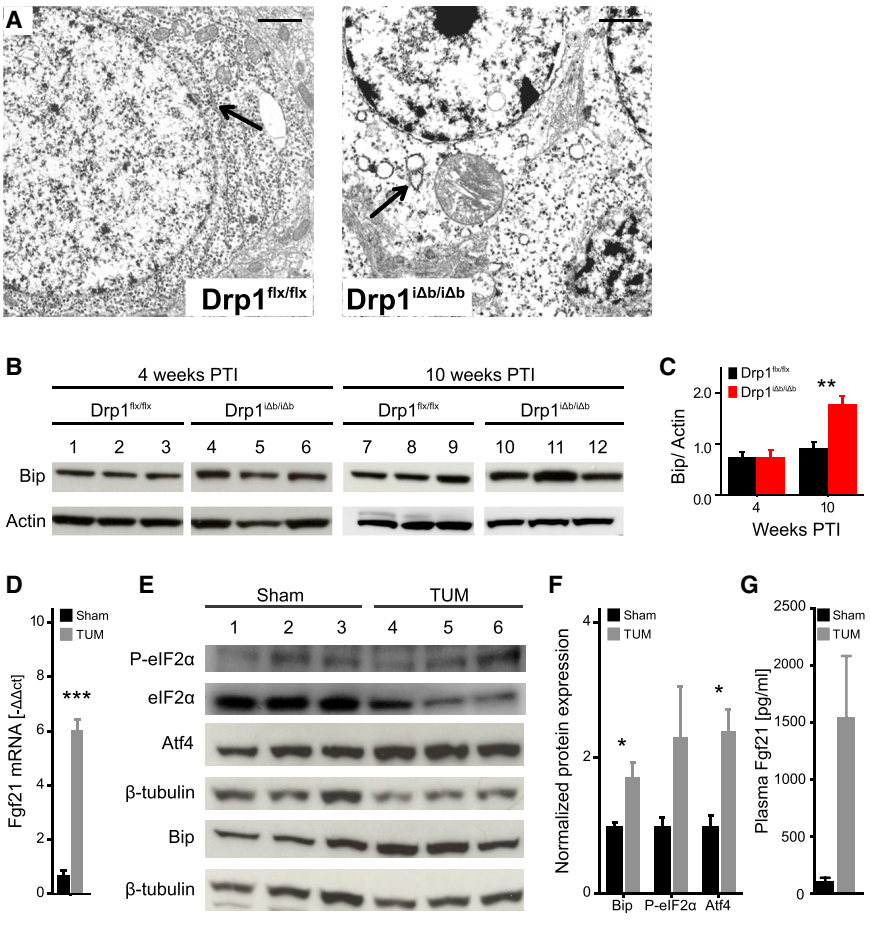

Figure 2. ER Stress Is Present and Sufficient for Fgf21 Induction upon *Drp1* Ablation

(A) Representative transmission electron microscopy (TEM) images of ER (marked by black arrows) of hippocampal neurons of 4-week-*Drp1*-ablated and control mice. Scale bar, 1 μm.

(B) Bip and actin western blot on hippocampal lysates of mice of the indicated genotypes at 10 weeks PTI. This experiment shares a loading control with Figure 1E.

(C) Quantification of Bip band intensity normalized to actin. Data represent average + SEM of at least 4 animals.

(D–G) Markers of ER stress and Fgf21 levels in brain tissue and plasma following intraventricular tunicamycin (TUM) injection.

(D) Fgf21 mRNA in TUM- and Sham-injected hippocampi.

(E and F) Representative western blot (E) and quantification (F) of TUM- and Sham-injected hippocampal lysates probed for the indicated proteins. Data represent average + SEM of at least 3 animals.

(G) Fgf21 plasma levels as determined by ELISA. Data represent average + SEM of at least 5 animals.

response to mitochondrial dysfunction (Bookout et al., 2013; Suomalainen et al., 2011; Fon Tacer et al., 2010) and that Fgf21 produced in the brain can cross the blood-brain barrier (BBB) to become detectable in plasma (Kharitonenkov and DiMarchi, 2015).

The ISR Is Activated upon Neuronal *Drp1* Ablation

We next wished to understand how mitochondrial dysfunction led to neuronal *Fgf21* transcription. Among the transcription factors known to control *Fgf21* expression, only *Atf4* was upregulated in *Drp1*-ablated brains (Figure S2A). *Atf4* translation is activated by phosphorylated eukaryotic translation initiation factor 2α (eIF2α), a crucial node in the ISR, responding to different forms of stress via decreased global translation and activation of transcriptional programs aimed at damage control (Donnelly et al., 2013). Western blot analysis confirmed Atf4 increase and eIF2α phosphorylation in $Drp1^{i\Delta b/i\Delta b}$ hippocampi (Figures 1E–1G). The canonical Atf4 target gene *Chop* (*Ddit3* or *Gadd153*) was accordingly upregulated in $Drp1^{i\Delta b/i\Delta b}$ hippocampus and cortex (Figure 1H). Furthermore, proteomics revealed that Atf4 target genes were significantly enriched in $Drp1^{i\Delta b/i\Delta b}$ brains (Figure S2B).

Four eIF2α kinases are capable of sensing specific ISR-triggering stress conditions: Perk responds to endoplasmic reticulum (ER) stress; Gcn2 acts as sensor for amino acid deficiency activated by uncharged tRNAs; Pkr senses double-stranded RNAs to signal viral infections and transduces the mitochondrial unfolded protein response (mtUPR) (Rath et al., 2012); and HRI becomes activated in the absence of heme (Donnelly et al., 2013). *In vivo*, the eIF2α-phosphorylating arm or arms of the ISR could not be detected by direct immunoblot (due to paucity of their expression and the mixed cellular nature of brain lysates). However, we investigated the specific upstream stress or stresses triggering the Fgf21-inducing cascade as a proxy for their respective ISR arm activation.

The close apposition of ER and mitochondria favors ER stress upon loss of proteins involved in mitochondrial and ER morphology regulation (de Brito and Scorrano, 2008; Muñoz et al., 2013). Drp1 was originally identified as a modulator of mitochondrial, as well as ER shape (Pitts et al., 1999; Yoon et al., 1998), suggesting that its deletion might also affect the ER. Electron microscopy (EM) of hippocampi 4 weeks PTI revealed that the ER was round and swollen, unlike the flat ER cisternae in the $Drp1^{flx/flx}$ counterparts (Figure 2A). In addition, the ER stress marker Bip/GRP78 was upregulated in $Drp1^{i\Delta b/i\Delta b}$ brains at later stages (Figures 2B and 2C), pointing to a link between neuronal *Drp1* deletion and ER stress activation. As a proof of principle, when we intraventricularly injected wild-type mice with the ER stress inducer tunicamycin, we noticed not only an activated unfolded protein response (UPR), as reflected by eIF2α phosphorylation and Atf4 elevation, but also an increase in *Fgf21* mRNA (Figures 2D–2F), leading to an elevation in plasma Fgf21 levels (Figure 2G). Altogether, these data indicate that $Drp1^{i\Delta b/i\Delta b}$ brains mount an UPR and that brain ER

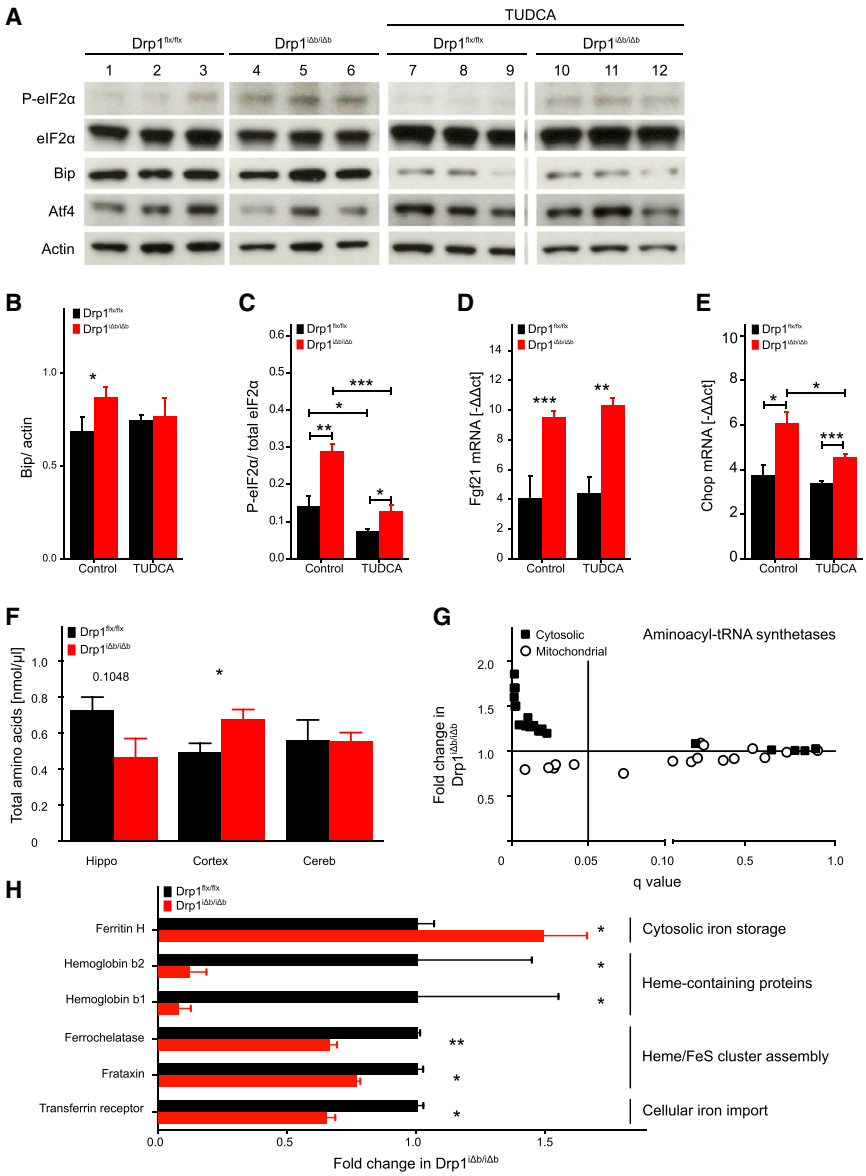

Figure 3. ER Stress-Independent ISR Branches Contribute to Fgf21 Induction

(A–E) Analysis of TUDCA-treated *Drp1*-ablated and control mice.

(A) Representative western blots of hippocampal lysates of the indicated genotype 10 weeks PTI, probed for Bip, P-eIF2α, total eIF2α, Atf4, and actin.

(B and C) Quantification of Bip (B) and phosphorylated eIF2α (C) band intensities normalized to actin (Bip) or total eIF2α, respectively.

(D and E) Hippocampal *Fgf21* (D) and *Chop* (E) mRNA expression determined by qRT-PCR, normalized to 18S rRNA ct values. Data represent average + SEM of at least 4 animals.

(F) Free amino acids in the indicated brain regions 10 weeks PTI. Data represent average ± SEM of at least 4 animals.

(G) Fold change in selected hits of a total proteomics screen 10 weeks PTI, plotted as a function of the respective q value.

(H) Fold change in selected, iron-related hits of a proteomics screen 10 weeks PTI.

Asterisks in (E) denote q values (i.e., p values adjusted for multiple testing): *$p < 0.05$, **$p < 0.01$, ***$p < 0.001$.

stress is sufficient to induce local Fgf21 expression and plasma Fgf21 elevation.

The ER Stress Component Is Dispensable for Fgf21 Induction

To understand whether ER stress was necessary to induce *Fgf21* expression, we capitalized on the orally bioavailable chemical chaperone tauroursodeoxycholic acid (TUDCA), which reduces mitochondria-induced ER stress in flies and mice (Debattisti et al., 2014; Muñoz et al., 2013). Co-treatment of $Drp1^{i\Delta b/i\Delta b}$ mice with TUDCA and tamoxifen resulted in lower Bip and P-eIF2α levels, confirming TUDCA bioavailability and activity in the brain. However, eIF2α phosphorylation and expression of *Fgf21*, as well as of the canonical Atf4 target gene *Chop*, remained elevated in TUDCA-treated $Drp1^{i\Delta b/i\Delta b}$ mice (Figures 3A–3E).

Overall, although ER stress is present in $Drp1^{i\Delta b/i\Delta b}$ brains and can cause *Fgf21* expression, its inhibition alone is not sufficient to abolish *Fgf21* in our model, suggesting that one or more of the alternative ISR branches contribute to the observed phenotype.

Impaired Amino Acid and Iron Metabolism Contributes to ISR-Driven Fgf21 Induction

To understand which mechanism accounted for Fgf21 production, we explored the role of the mitochondrial bioenergetics defect caused by *Drp1* ablation (Oettinghaus et al., 2016). However, at 10 weeks PTI, protein levels of Hsp60 and mRNA levels of *Hsp10*, *ClpP*, and *Yme1l*, markers of the mtUPR, were normal in $Drp1^{i\Delta b/i\Delta b}$ brains (Figures S3A–S3C). We confirmed this by an unbiased proteomic analysis on pooled hippocampi and cortices from mice 10 weeks PTI: mtUPR was not in place in $Drp1^{i\Delta b/i\Delta b}$ mice, with three of the five acknowledged mtUPR genes even significantly decreased (Figure S3D).

Alternatively, ISR could result from a defect in amino acid biosynthesis or catabolism, both crucially located at the mitochondrial level. Total amino acid content was moderately decreased in the hippocampus, whereas amino acids were significantly increased in the cortex of $Drp1^{i\Delta b/i\Delta b}$ mice (Figure 3F). In addition, aminoacyl-tRNA synthetases were significantly enriched hits of the proteomics analysis of $Drp1^{i\Delta b/i\Delta b}$ brains. Even more remarkable was the signature

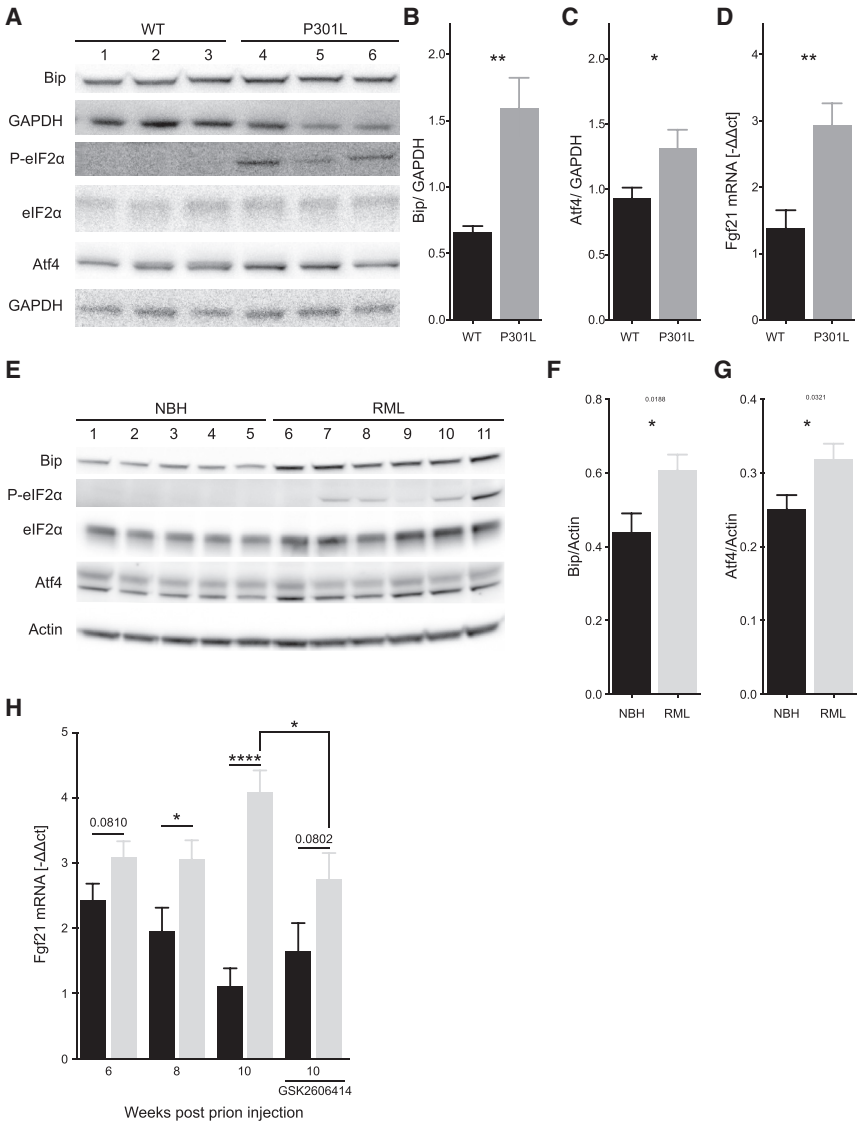

Figure 4. Brain-Derived Fgf21 Is Induced in Mouse Models of Neurodegeneration

Data from P301L tau mutant mice (A–D) and RML prion inoculation disease model (E–H).

(A) Western blot of hippocampi of 9-month-old P301L mutant mice and age-matched controls.

(B and C) Quantification of Bip (B) and Atf4 (C) band intensities, normalized to their respective loading control.

(D) Hippocampal *Fgf21* mRNA expression of 9-month-old P301L mutant mice and age-matched controls, determined by qRT-PCR. Data represent average + SEM of at least 4 animals.

(E) Western blot of hippocampi of mice intracerebrally inoculated with RML prions at 10 weeks postinoculation (wpi).

(F and G) Quantification of Bip (F) and Atf4 (G) band intensities normalized to their respective loading control.

(H) Fgf21 transcript levels in hippocampi of normal brain homogenate (NBH) or RML prion-inoculated mice at 6, 8, and 10 wpi. Data represent average + SEM of at least 8 animals.

of the subcellular distribution of the altered aminoacyl-tRNA synthetases: 80% of cytosolic aminoacyl-tRNA synthetases were significantly upregulated in *Drp1*$^{i\Delta b/i\Delta b}$ brains, while their mitochondrial counterparts were mostly downregulated (Figure 3G). Because heme biosynthesis depends on amino acid metabolism, as well as on mitochondrial function (Lane et al., 2015), we next wanted to check its potential involvement in the phenotype. Ferrochelatase, a rate-limiting mitochondria-localized component of the heme biosynthetic pathway, was downregulated in *Drp1*$^{i\Delta b/i\Delta b}$ mice, as was mitochondrial matrix iron metabolism regulator frataxin (Figure 3H). Accordingly, cytosolic iron storage protein ferritin H was upregulated, and iron importer transferrin receptor was downregulated in *Drp1*$^{i\Delta b/i\Delta b}$ brains. Finally, heme-containing hemoglobin was also strongly downregulated in *Drp1*$^{i\Delta b/i\Delta b}$ brains (Figure 3H), reflecting the global changes in iron metabolism caused by Drp1 ablation. Altogether, these data suggest that both amino acid metabolism and heme biosynthesis are altered upon *Drp1* ablation and may contribute to ISR activation in *Drp1*$^{i\Delta b/i\Delta b}$ mice.

Brain-Derived Fgf21 Is Induced in Two Etiologically Distinct Mouse Models of Neurodegeneration

We next wished to investigate the possibility that Fgf21 was induced in clinically relevant models of brain pathologies affecting mitochondrial dynamics and function. To this end, we examined tau-mutated P301L mice, a model of frontotemporal dementia (FTD) (Lewis et al., 2000), as well as the tg37-Rocky Mountain Laboratory (RML) prion inoculation model (Mallucci et al., 2003; Moreno et al., 2013). Both models display ISR that responds to PERK inhibition (Moreno et al., 2013; Radford et al., 2015), as well as defects in mitochondrial function and transport (Choi et al., 2014; Chou et al., 2011). In both models, the ER stress and ISR activation markers Bip, P-eIF2α, and Atf4 were upregulated (Figures 4A–4C, 4E, and 4F). *Fgf21* mRNA was elevated in hippocampi of P301L, as well as of prion-injected mice at different time points, also before the onset of symptoms (Figures 4D and 4H). Prion-inoculated mice orally treated with PERK inhibitor GSK2606414 showed a demonstrable decrease in Fgf21 expression, confirming that Fgf21 induction is ER stress dependent (Figure 4H). Thus, *Fgf21* transcription is induced in etiologically distinct mouse models of neurodegeneration not caused by a primary mitochondrial defect. Our data collectively indicate that Fgf21 might be an early biomarker for neurodegenerative processes associated with mitochondrial dysfunction and ISR activation.

DISCUSSION

Here, we report that *Drp1* deletion from adult forebrain neurons *in vivo* triggers the activation of a multi-branched stress response culminating in brain *Fgf21* expression. Impaired mitochondrial function is linked to Fgf21 production in various peripheral tissues, but not in brain (Cornu et al., 2014; Guridi et al., 2015; Hagiwara et al., 2012; Keipert et al., 2014; Kim et al., 2013a, 2013b; Touvier et al., 2015; Tyynismaa et al., 2010). In our system, *Drp1* deletion impairs mitochondrial dynamics and ER morphology and induces ER stress (Figure 2). This could be due to alterations in mitochondria-ER contacts affecting the two organellar membranes, modifying membrane curvature and activating ER stress sensor PERK (Volmer et al., 2013), or due to direct Drp1 action on ER shape (Yoon et al., 1998). Lack of rescue by TUDCA treatment (Figures 3A–3E) indicates that additional stress pathways converging on eIF2α are activated in the brain upon Drp1 deletion. In particular, heme biosynthesis and amino acid metabolism, two mitochondria-related pathways, are affected by brain *Drp1* ablation (Figures 3F–3H). Heme biosynthesis is a partially mitochondria-resident pathway that requires iron to be actively imported into the organelles, as well as amino acids as precursors. Therefore, given the compromised bioenergetic state of Drp1-ablated mitochondria, which could affect organellar iron import, it is plausible that intramitochondrial steps of heme biosynthesis are impaired. This is corroborated by the increase in cytosolic ferritin H and the decrease in transferrin receptor (a signature of high cytosolic iron) (Muckenthaler et al., 2008). The stark decrease of two hemoglobin subunits, which would bind heme, is also in line with the heme deprivation hypothesis (Figure 3H) (Chen, 2007; Han et al., 2001).

Different brain regions display differential sensitivity to *Drp1* deletion, reflecting their individual metabolic needs and responses (Berthet et al., 2014; Kageyama et al., 2012; Oettinghaus et al., 2016; Shields et al., 2015). One explanation can lie in the ability of Atf4 to act with other transcription factors in a combinatorial manner based on the nature of the stress (Kilberg et al., 2009). Total amino acid concentration varied drastically between hippocampus and cortex (Figure 3F), which could be linked to the presence, in the anterior piriform cortex, of the body's amino acid deficiency sensor (Anthony and Gietzen, 2013). It is therefore conceivable that the differential sensitivity to Drp1 ablation is linked to the different degrees of amino acid concentration changes within the brain.

The importance of Fgf21 as a proxy of brain mitochondrial defects is reinforced by the finding that *Fgf21* is expressed in brains of prion-inoculated mice, as well as of mice carrying the FTD-associated P301L tau mutation (Figures 4D and 4H). Similar to *Drp1*-deleted mice, both models display defects in mitochondrial function and transport, as well as ER stress-dependent ISR activation that can be reversed by PERK blockage (Chou et al., 2011; Radford et al., 2015). Although dysregulated iron and heme have also been linked to tau accumulation and prion diseases (Belaidi and Bush, 2016; Singh, 2014), ISR activation in these models is exclusively PERK dependent, which makes them an ideal model to study the reversal of Fgf21 expression by GSK2606414.

Fgf21 is regulated by circadian and nutritional factors (Fisher and Maratos-Flier, 2016; Kharitonenkov and DiMarchi, 2017), potentially limiting the specificity of its detection *in vivo* as a biomarker of neuronal mitochondrial dysfunction. In particular, liver Fgf21 production is modulated by diverse dietary manipulations beyond fasting (Fisher and Maratos-Flier, 2016). For these reasons, the exploration of Fgf21 levels in patients' samples was beyond the scope of this work. Nevertheless, in light of our findings and of Fgf21 being a biomarker of mitochondrial myopathies, we encourage clinicians to explore this possibility in existing, appropriately controlled patient cohorts. Of course, confounding factors such as diabetes, obesity, or liver disease shall be carefully considered. To this end, cerebrospinal fluid (CSF) analyses might prove relevant, although at least upon its acute peripheral injection in mice, this cytokine can also cross the BBB (Douris et al., 2015; Hsuchou et al., 2007).

Future work grounded in the discoveries reported here will test whether Fgf21 is induced in other diseases sharing mitochondrial and ER stress components, like Parkinson's disease and disorders of the amyotrophic lateral sclerosis/FTD spectrum (Stoica et al., 2014; Wang et al., 2016a, 2016b). While we do not expect Fgf21 to aid in the diagnostic discrimination of different neurodegenerative entities, we can predict that our discovery of a secreted, brain-derived factor induced in etiologically diverse CNS diseases would represent a much-needed progress in presymptomatic screening, within a combined framework of validated biomarkers and predictive algorithms.

In conclusion, our work shows that neurons sense dysregulated mitochondrial dynamics and ER stress to activate a multi-branched stress response culminating in the release of Fgf21. The same Fgf21 mitokine is produced in the brains of bona fide tauopathy and prion disease mouse models, highlighting its potential as a marker of brain mitochondrial dysfunction.

EXPERIMENTAL PROCEDURES

For more details, refer to the Supplemental Experimental Procedures.

Mice

Drp1$^{i\Delta b/i\Delta b}$ and tau mutant (P301L) mice were described previously (Oettinghaus et al., 2016; Lewis et al., 2000; Radford et al., 2015). For the prion disease model, hemizygous tg37 mice inoculated with RML prion were used (Mallucci et al., 2003; Moreno et al., 2013).

Western Blot

Lysates of perfused mouse brains were analyzed as previously described (Oettinghaus et al., 2016). Antibodies are listed in Supplemental Experimental Procedures.

Real-Time PCR

Organs were collected from PBS-perfused mice and RNA was isolated (RNeasy kits 74104, 74704, and 74804). RT-PCR was performed using the High Capacity cDNA Reverse Transcription Kit (Invitrogen, 4368814). Real-time PCR was performed using TaqMan assays (Life Technologies) on a 7900HT Real-Time PCR System (Applied Biosystems). TaqMan assays are listed in Supplemental Experimental Procedures. Cross-threshold (ct) values were normalized to 18S ct values.

Fluorescent Detection of *Fgf21* mRNA

This analysis was performed as a service by Advanced Cell Diagnostics with the RNAscope technology, following the standard manufacturer's protocol.

ELISA

Blood was collected between 9 and 10 a.m., and plasma Fgf21 levels were analyzed according to the manufacturer's instructions (BioVendor, RD291108200R).

Quantitative Proteomics

Details on this analysis were described previously (Oettinghaus et al., 2016). Data are available via ProteomeXchange: PXD004890.

Statistics

Data analysis was performed with GraphPad Prism 6. For statistical analyses, two-tailed Student's t test and one-way ANOVA with Sidak's multiple comparison corrections were used. Unless otherwise specified, asterisks denote p values of an unpaired, two-tailed Student's t test: *$p < 0.05$, **$p < 0.01$, ***$p < 0.001$, ****$p < 0.0001$.

SUPPLEMENTAL INFORMATION

Supplemental Information includes Supplemental Experimental Procedures and three figures and can be found with this article online at https://doi.org/10.1016/j.celrep.2018.07.023.

ACKNOWLEDGMENTS

The authors thank M. Dürrenberger (Microscopy Center Biozentrum, University of Basel), the staff of the Microscopy Core Facility at the Department of Biomedicine (University of Basel), and M. Baumann (Institute of Pathology, Basel University Hospitals) for their expert help with experimental procedures. This work was supported by the SNSF (31003A_127308), Novartis Foundation for Medical-Biological Research, Desirée and Nils Yde Foundation (420-14), Bangerter-Rhyner Foundation (8472/HEG-DSV), Nora van Meeuwen-Haefliger Foundation, and Mach-Gaensslen Foundation (to S.F.); Forschungsfonds of Basel University (to L.M.R. and B.O.); ERC (grant UPR Neuro; 282280), MRC, Alzheimer's Society, and ARUK/DRI (to G.M.); and Telethon Italy (GGP12162 and GPP10005), AIRC Italy (IG15748), ERC ERMITO, FP7 CIG CristOpa (PCIG13-GA-2013-618697), and MIUR FIRB Automed (RBAP11-Z3YA_005 to L.S.).

AUTHOR CONTRIBUTIONS

L.M.R., B.O., M.H., M.L., C.A., L.S., C.S., A.N., and A.S. performed experiments. L.M.R., B.O., J.H., M.T., A.S., and A.E. analyzed and interpreted experimental data. G.M., L.S., and S.F. conceived the project and coordinated and supervised research. L.M.R., B.O., L.S., and S.F. wrote the manuscript.

DECLARATION OF INTERESTS

The authors declare no competing interests.

Received: September 21, 2016
Revised: April 23, 2018
Accepted: July 6, 2018
Published: August 7, 2018

REFERENCES

Anthony, T.G., and Gietzen, D.W. (2013). Detection of amino acid deprivation in the central nervous system. Curr. Opin. Clin. Nutr. Metab. Care *16*, 96–101.

Belaidi, A.A., and Bush, A.I. (2016). Iron neurochemistry in Alzheimer's disease and Parkinson's disease: targets for therapeutics. J. Neurochem. *139* (*Suppl 1*), 179–197.

Berthet, A., Margolis, E.B., Zhang, J., Hsieh, I., Zhang, J., Hnasko, T.S., Ahmad, J., Edwards, R.H., Sesaki, H., Huang, E.J., and Nakamura, K. (2014). Loss of mitochondrial fission depletes axonal mitochondria in midbrain dopamine neurons. J. Neurosci. *34*, 14304–14317.

Bookout, A.L., de Groot, M.H., Owen, B.M., Lee, S., Gautron, L., Lawrence, H.L., Ding, X., Elmquist, J.K., Takahashi, J.S., Mangelsdorf, D.J., and Kliewer, S.A. (2013). FGF21 regulates metabolism and circadian behavior by acting on the nervous system. Nat. Med. *19*, 1147–1152.

Chen, J.J. (2007). Regulation of protein synthesis by the heme-regulated eIF2α kinase: relevance to anemias. Blood *109*, 2693–2699.

Choi, H.S., Choi, Y.G., Shin, H.Y., Oh, J.M., Park, J.H., Kim, J.I., Carp, R.I., Choi, E.K., and Kim, Y.S. (2014). Dysfunction of mitochondrial dynamics in the brains of scrapie-infected mice. Biochem. Biophys. Res. Commun. *448*, 157–162.

Chou, J.L., Shenoy, D.V., Thomas, N., Choudhary, P.K., Laferla, F.M., Goodman, S.R., and Breen, G.A. (2011). Early dysregulation of the mitochondrial proteome in a mouse model of Alzheimer's disease. J. Proteomics *74*, 466–479.

Cornu, M., Oppliger, W., Albert, V., Robitaille, A.M., Trapani, F., Quagliata, L., Fuhrer, T., Sauer, U., Terracciano, L., and Hall, M.N. (2014). Hepatic mTORC1 controls locomotor activity, body temperature, and lipid metabolism through FGF21. Proc. Natl. Acad. Sci. USA *111*, 11592–11599.

de Brito, O.M., and Scorrano, L. (2008). Mitofusin 2 tethers endoplasmic reticulum to mitochondria. Nature *456*, 605–610.

Debattisti, V., Pendin, D., Ziviani, E., Daga, A., and Scorrano, L. (2014). Reduction of endoplasmic reticulum stress attenuates the defects caused by *Drosophila* mitofusin depletion. J. Cell Biol. *204*, 303–312.

Degirolamo, C., Sabbà, C., and Moschetta, A. (2016). Therapeutic potential of the endocrine fibroblast growth factors FGF19, FGF21 and FGF23. Nat. Rev. Drug Discov. *15*, 51–69.

Donnelly, N., Gorman, A.M., Gupta, S., and Samali, A. (2013). The eIF2α kinases: their structures and functions. Cell. Mol. Life Sci. *70*, 3493–3511.

Douris, N., Stevanovic, D.M., Fisher, F.M., Cisu, T.I., Chee, M.J., Nguyen, N.L., Zarebidaki, E., Adams, A.C., Kharitonenkov, A., Flier, J.S., et al. (2015). Central fibroblast growth factor 21 browns white fat via sympathetic action in male mice. Endocrinology *156*, 2470–2481.

DuBoff, B., Feany, M., and Götz, J. (2013). Why size matters—balancing mitochondrial dynamics in Alzheimer's disease. Trends Neurosci. *36*, 325–335.

Fisher, F.M., and Maratos-Flier, E. (2016). Understanding the physiology of FGF21. Annu. Rev. Physiol. *78*, 223–241.

Fon Tacer, K., Bookout, A.L., Ding, X., Kurosu, H., John, G.B., Wang, L., Goetz, R., Mohammadi, M., Kuro-o, M., Mangelsdorf, D.J., and Kliewer, S.A. (2010). Research resource: comprehensive expression atlas of the fibroblast growth factor system in adult mouse. Mol. Endocrinol. *24*, 2050–2064.

Guridi, M., Tintignac, L.A., Lin, S., Kupr, B., Castets, P., and Rüegg, M.A. (2015). Activation of mTORC1 in skeletal muscle regulates whole-body metabolism through FGF21. Sci. Signal. *8*, ra113.

Hagiwara, A., Cornu, M., Cybulski, N., Polak, P., Betz, C., Trapani, F., Terracciano, L., Heim, M.H., Rüegg, M.A., and Hall, M.N. (2012). Hepatic mTORC2 activates glycolysis and lipogenesis through Akt, glucokinase, and SREBP1c. Cell Metab. *15*, 725–738.

Han, A.P., Yu, C., Lu, L., Fujiwara, Y., Browne, C., Chin, G., Fleming, M., Leboulch, P., Orkin, S.H., and Chen, J.J. (2001). Heme-regulated eIF2α kinase (HRI) is required for translational regulation and survival of erythroid precursors in iron deficiency. EMBO J. *20*, 6909–6918.

Hsuchou, H., Pan, W., and Kastin, A.J. (2007). The fasting polypeptide FGF21 can enter brain from blood. Peptides *28*, 2382–2386.

Ishihara, N., Nomura, M., Jofuku, A., Kato, H., Suzuki, S.O., Masuda, K., Otera, H., Nakanishi, Y., Nonaka, I., Goto, Y., et al. (2009). Mitochondrial fission factor Drp1 is essential for embryonic development and synapse formation in mice. Nat. Cell Biol. *11*, 958–966.

Kageyama, Y., Zhang, Z., Roda, R., Fukaya, M., Wakabayashi, J., Wakabayashi, N., Kensler, T.W., Reddy, P.H., Iijima, M., and Sesaki, H. (2012). Mitochondrial division ensures the survival of postmitotic neurons by suppressing oxidative damage. J. Cell Biol. *197*, 535–551.

Keipert, S., Ost, M., Johann, K., Imber, F., Jastroch, M., van Schothorst, E.M., Keijer, J., and Klaus, S. (2014). Skeletal muscle mitochondrial uncoupling

drives endocrine cross-talk through the induction of FGF21 as a myokine. Am. J. Physiol. Endocrinol. Metab. *306*, E469–E482.

Kharitonenkov, A., and DiMarchi, R. (2015). FGF21 revolutions: recent advances illuminating FGF21 biology and medicinal properties. Trends Endocrinol. Metab. *26*, 608–617.

Kharitonenkov, A., and DiMarchi, R. (2017). Fibroblast growth factor 21 night watch: advances and uncertainties in the field. J. Intern. Med. *281*, 233–246.

Kilberg, M.S., Shan, J., and Su, N. (2009). ATF4-dependent transcription mediates signaling of amino acid limitation. Trends Endocrinol. Metab. *20*, 436–443.

Kim, K.H., Jeong, Y.T., Oh, H., Kim, S.H., Cho, J.M., Kim, Y.N., Kim, S.S., Kim, D.H., Hur, K.Y., Kim, H.K., et al. (2013a). Autophagy deficiency leads to protection from obesity and insulin resistance by inducing Fgf21 as a mitokine. Nat. Med. *19*, 83–92.

Kim, K.H., Jeong, Y.T., Kim, S.H., Jung, H.S., Park, K.S., Lee, H.Y., and Lee, M.S. (2013b). Metformin-induced inhibition of the mitochondrial respiratory chain increases FGF21 expression via ATF4 activation. Biochem. Biophys. Res. Commun. *440*, 76–81.

Lane, D.J., Merlot, A.M., Huang, M.L., Bae, D.H., Jansson, P.J., Sahni, S., Kalinowski, D.S., and Richardson, D.R. (2015). Cellular iron uptake, trafficking and metabolism: key molecules and mechanisms and their roles in disease. Biochim. Biophys. Acta *1853*, 1130–1144.

Lewis, J., McGowan, E., Rockwood, J., Melrose, H., Nacharaju, P., Van Slegtenhorst, M., Gwinn-Hardy, K., Paul Murphy, M., Baker, M., Yu, X., et al. (2000). Neurofibrillary tangles, amyotrophy and progressive motor disturbance in mice expressing mutant (P301L) tau protein. Nat. Genet. *25*, 402–405.

Mallucci, G., Dickinson, A., Linehan, J., Klöhn, P.C., Brandner, S., and Collinge, J. (2003). Depleting neuronal PrP in prion infection prevents disease and reverses spongiosis. Science *302*, 871–874.

Moreno, J.A., Halliday, M., Molloy, C., Radford, H., Verity, N., Axten, J.M., Ortori, C.A., Willis, A.E., Fischer, P.M., Barrett, D.A., and Mallucci, G.R. (2013). Oral treatment targeting the unfolded protein response prevents neurodegeneration and clinical disease in prion-infected mice. Sci. Transl. Med. *5*, 206ra138.

Muckenthaler, M.U., Galy, B., and Hentze, M.W. (2008). Systemic iron homeostasis and the iron-responsive element/iron-regulatory protein (IRE/IRP) regulatory network. Annu. Rev. Nutr. *28*, 197–213.

Muñoz, J.P., Ivanova, S., Sánchez-Wandelmer, J., Martínez-Cristóbal, P., Noguera, E., Sancho, A., Díaz-Ramos, A., Hernández-Alvarez, M.I., Sebastián, D., Mauvezin, C., et al. (2013). Mfn2 modulates the UPR and mitochondrial function via repression of PERK. EMBO J. *32*, 2348–2361.

Oettinghaus, B., Schulz, J.M., Restelli, L.M., Licci, M., Savoia, C., Schmidt, A., Schmitt, K., Grimm, A., Morè, L., Hench, J., et al. (2016). Synaptic dysfunction, memory deficits and hippocampal atrophy due to ablation of mitochondrial fission in adult forebrain neurons. Cell Death Differ. *23*, 18–28.

Pernas, L., and Scorrano, L. (2016). Mito-morphosis: mitochondrial fusion, fission, and cristae remodeling as key mediators of cellular function. Annu. Rev. Physiol. *78*, 505–531.

Pitts, K.R., Yoon, Y., Krueger, E.W., and McNiven, M.A. (1999). The dynamin-like protein DLP1 is essential for normal distribution and morphology of the endoplasmic reticulum and mitochondria in mammalian cells. Mol. Biol. Cell *10*, 4403–4417.

Radford, H., Moreno, J.A., Verity, N., Halliday, M., and Mallucci, G.R. (2015). PERK inhibition prevents tau-mediated neurodegeneration in a mouse model of frontotemporal dementia. Acta Neuropathol. *130*, 633–642.

Rath, E., Berger, E., Messlik, A., Nunes, T., Liu, B., Kim, S.C., Hoogenraad, N., Sans, M., Sartor, R.B., and Haller, D. (2012). Induction of dsRNA-activated protein kinase links mitochondrial unfolded protein response to the pathogenesis of intestinal inflammation. Gut *61*, 1269–1278.

Shields, L.Y., Kim, H., Zhu, L., Haddad, D., Berthet, A., Pathak, D., Lam, M., Ponnusamy, R., Diaz-Ramirez, L.G., Gill, T.M., et al. (2015). Dynamin-related protein 1 is required for normal mitochondrial bioenergetic and synaptic function in CA1 hippocampal neurons. Cell Death Dis. *6*, e1725.

Singh, N. (2014). The role of iron in prion disease and other neurodegenerative diseases. PLoS Pathog. *10*, e1004335.

Stoica, R., De Vos, K.J., Paillusson, S., Mueller, S., Sancho, R.M., Lau, K.F., Vizcay-Barrena, G., Lin, W.L., Xu, Y.F., Lewis, J., et al. (2014). ER-mitochondria associations are regulated by the VAPB-PTPIP51 interaction and are disrupted by ALS/FTD-associated TDP-43. Nat. Commun. *5*, 3996.

Suomalainen, A., Elo, J.M., Pietiläinen, K.H., Hakonen, A.H., Sevastianova, K., Korpela, M., Isohanni, P., Marjavaara, S.K., Tyni, T., Kiuru-Enari, S., et al. (2011). FGF-21 as a biomarker for muscle-manifesting mitochondrial respiratory chain deficiencies: a diagnostic study. Lancet Neurol. *10*, 806–818.

Tezze, C., Romanello, V., Desbats, M.A., Fadini, G.P., Albiero, M., Favaro, G., Ciciliot, S., Soriano, M.E., Morbidoni, V., Cerqua, C., et al. (2017). Age-associated loss of OPA1 in muscle impacts muscle mass, metabolic homeostasis, systemic inflammation, and epithelial senescence. Cell Metab. *25*, 1374–1389.e6.

Touvier, T., De Palma, C., Rigamonti, E., Scagliola, A., Incerti, E., Mazelin, L., Thomas, J.L., D'Antonio, M., Politi, L., Schaeffer, L., et al. (2015). Muscle-specific Drp1 overexpression impairs skeletal muscle growth via translational attenuation. Cell Death Dis. *6*, e1663.

Twig, G., Hyde, B., and Shirihai, O.S. (2008). Mitochondrial fusion, fission and autophagy as a quality control axis: the bioenergetic view. Biochim. Biophys. Acta *1777*, 1092–1097.

Tyynismaa, H., Carroll, C.J., Raimundo, N., Ahola-Erkkilä, S., Wenz, T., Ruhanen, H., Guse, K., Hemminki, A., Peltola-Mjøsund, K.E., Tulkki, V., et al. (2010). Mitochondrial myopathy induces a starvation-like response. Hum. Mol. Genet. *19*, 3948–3958.

Volmer, R., van der Ploeg, K., and Ron, D. (2013). Membrane lipid saturation activates endoplasmic reticulum unfolded protein response transducers through their transmembrane domains. Proc. Natl. Acad. Sci. USA *110*, 4628–4633.

Wai, T., and Langer, T. (2016). Mitochondrial dynamics and metabolic regulation. Trends Endocrinol. Metab. *27*, 105–117.

Wakabayashi, J., Zhang, Z., Wakabayashi, N., Tamura, Y., Fukaya, M., Kensler, T.W., Iijima, M., and Sesaki, H. (2009). The dynamin-related GTPase Drp1 is required for embryonic and brain development in mice. J. Cell Biol. *186*, 805–816.

Wang, W., Wang, L., Lu, J., Siedlak, S.L., Fujioka, H., Liang, J., Jiang, S., Ma, X., Jiang, Z., da Rocha, E.L., et al. (2016a). The inhibition of TDP-43 mitochondrial localization blocks its neuronal toxicity. Nat. Med. *22*, 869–878.

Wang, W., Wang, X., Fujioka, H., Hoppel, C., Whone, A.L., Caldwell, M.A., Cullen, P.J., Liu, J., and Zhu, X. (2016b). Parkinson's disease-associated mutant VPS35 causes mitochondrial dysfunction by recycling DLP1 complexes. Nat. Med. *22*, 54–63.

Yoon, Y., Pitts, K.R., Dahan, S., and McNiven, M.A. (1998). A novel dynamin-like protein associates with cytoplasmic vesicles and tubules of the endoplasmic reticulum in mammalian cells. J. Cell Biol. *140*, 779–793.

Cell Reports, Volume *24*

Supplemental Information

Neuronal Mitochondrial Dysfunction Activates the Integrated Stress Response to Induce Fibroblast Growth Factor 21

Lisa Michelle Restelli, Björn Oettinghaus, Mark Halliday, Cavit Agca, Maria Licci, Lara Sironi, Claudia Savoia, Jürgen Hench, Markus Tolnay, Albert Neutzner, Alexander Schmidt, Anne Eckert, Giovanna Mallucci, Luca Scorrano, and Stephan Frank

SUPPLEMENTARY EXPERIMENTAL PROCEDURES

Mice. Generation of tamoxifen-inducible, forebrain neuron-specific Drp1$^{flx/flx}$ Cre^{+} mice was described recently (Oettinghaus et al., 2016). At 8 weeks of age recombination of the floxed loci was induced by tamoxifen injection (Sigma Aldrich, Germany; 1mg twice daily for 5 consecutive days). For genotyping, genomic DNA was isolated from tail tips by proteinase K digestion (Sigma Aldrich, Germany). CreERT2 transgene was amplified using the following primers: 5' GGT TCT CCG TTT GCA CTC AGG A 3', 5' CTG CAT GCA CGG GAC AGC TCT 3', 5' GCT TGC AGG TAC AGG AGG TAG T 3'. Recombination of the Drp1 locus was detected using the following primers: 5' CAG CTG CAC TGG CTT CAT GAC TC 3', 5' TGC CAA GAA TGA TTA CAG TCA GG 3'.

Mutant tau (P301L) and prion-injected (RML) mice have been described elsewhere (Moreno et al., 2013; Radford et al., 2015). When indicated, mice were treated orally with PERK inhibitor GSK2606414 (50mg/kg, three doses, starting at 10 wpi; Moreno et al., 2013).

For intraventricular tunicamycin microinjections, mice were anaesthetized by i.p. injection of 10 mg/kg ketamine and 20 mg/kg xylazine. Injections were performed with a 10 µl Hamilton microsyringe as described (Ono et al., 2012) using -0.5 mm posterior, -1.0 mm lateral, -2.0 mm inferior relative to bregma as coordinates. 2 µl of 0.1 µg/µl tunicamycin in 1% DMSO or 2 µl vehicle were carefully injected over the course of 2 min and the needle left in place for 5 min before retraction. Following scalp suture mice were monitored until recovery from anesthesia. After 48h, mice were sacrificed, their hippocampi dissected and plasma collected (between 9 and 10 AM).

TUDCA treatment was initiated at day 1 PTI. Mice were fed 0.4% TUDCA-supplemented chow (chow: ssniff, Germany; TUDCA: Merck, UK) for 7 weeks.

All experiments were performed under specific pathogen-free conditions, in accordance with Swiss animal protection legislation and with approval of the Basel Veterinary Committee for Animal Care (permits 2393, 23288).

Western Blot. Lysates of perfused mouse brains were analyzed as previously described (Oettinghaus et al., 2016). Membranes were probed with the following antibodies: Drp1 (BD Biosciences; 611112), Atf4 (Santa Cruz; sc-200), Bip (BD Biosciences; 610978), eIF2α total (Cell Signaling Technology, #5324), eIF2α phospho-Ser51 (Cell Signaling Technology, #3398), Hsp60 (Enzo; ADI-SPA-807-E), actin (Thermo

Scientific; MA1-91399), GAPDH (Abnova; H00002597-M03) and beta-tubulin (Sigma; T8660). Secondary antibodies were anti mouse-HRP (GE Healthcare; NA931) and anti-rabbit-HRP (GE Healthcare; NA934); for signal detection Amersham ECL Prime Western Blotting Detection Reagent (GE Healthcare; RPN2232) was used in conjunction with Amersham Hyperfilm (GE Healthcare; 28-9068-44), or with an Azure C300 imager (Azure Biosystems, USA). Densitometry was performed using ImageJ.

Histology and immunohistochemistry. Following transcardial formaldehyde perfusion of anaesthetized mice, histological assessment was performed using previously described protocols (Oettinghaus et al., 2016).

In brief, coronal hippocampal sections (4 μm) were prepared from formalin-fixed, paraffin-embedded (FFPE) wildtype mouse brain and hematoxylin-eosin stained using standard protocols. In addition, FFPE sections were subjected to immunohistochemistry using anti-GFAP (DAKO; 1:500), anti-NeuN (Chemicon; 1:200), and anti-Iba1 (Wako; 1:3000); secondary antibody was anti-rabbit IgG (Vector; ImmPRESS Reagent Kit). All immunohistochemical stains were performed on an automated Ventana immunostaining instrument using prediluted antibodies (Ventana Medical Systems Inc.).

Fluorescent detection of Fgf21 mRNA. This analysis was performed as a service by Advanced Cell Diagnostics, Inc. with the RNAscope technology, following standard manufacturer's protocol. Briefly, frozen mouse brain sections (10μm) were stained with probes targeting Fgf21, Aldh1l1 (astrocytes) and RBfox3 (also known as NeuN, neurons) mRNAs. POLR2A/PPIB/UBC were used as a positive control marker for sample quality control and to evaluate RNA quality in both tissue samples. Bacterial gene dapB was used as a negative control. Images were acquired on a Zeiss LSM 510 Meta confocal microscope.

For quantification of Fgf21 signal, Fgf21-positive area/ total area was employed within the CA1 region. Briefly, images were thresholded and analyzed with the "analyze particles" function on ImageJ within an indicated ROI corresponding to the CA1 region.

Ultrastructural analyses. Transmission electron microscopy was performed as previously described (Oettinghaus et al., 2016) using a Phillips CM100 transmission electron microscope.

Real-time PCR. Organs were collected from PBS-perfused mice and RNA was isolated (RNeasy Lipid Tissue Kit for adipose tissue, 74804; RNeasy Fibrous Tissue kit for muscle, 74704; RNeasy kit for other organs, 74104; all from Qiagen). Reverse-transcriptase PCR was performed using the High Capacity cDNA Reverse Transcription Kit (Invitrogen; 4368814). Real-time PCR was performed using TaqMan assays (Life Technologies) on a 7900HT Real-Time PCR System (Applied Biosystems). The following Taqman assays were used: FGF21 (Mm00840165_g1), 18S (Mm03928990_g1), Chop (Mm01135937_g1), PPARα (m00440939_m1), PPARδ (Mm00803184_m1), PGC-1α (Mm01208835_m1), PGC-1β (Mm00504720_m1), ATF4 (Mm00515325_g1), Akt1 (Mm01331626_m1), PI3K (Mm00803160_m1), Hsp10 (Mm00434083_m1), Clpp (Mm00489940_m1), Yme1l1 (Mm00496843_m1). Cross-threshold (ct) values were normalized to 18S ct values.

ELISA and other kits. Blood was collected between 9 and 10 AM in EDTA-coated tubes and hormone levels were detected by ELISA from plasma (FGF21: BioVendor, RD291108200R). Total amino acids were measured on hippocampi, cortices and cerebella 10 weeks PTI with the L-Amino Acid Quantitation Kit (MAK002, Sigma Aldrich, Germany) according to manufacturer's instructions.

Proteomics. In Fig. S2B, P-values denote likelihood of protein group being a random sample of the total population of detected proteins (Fisher's exact test). Reference dataset was obtained from (Han et al., 2013).

SUPPLEMENTARY FIGURE LEGENDS

Fig. S1 Cytoarchitecture of hippocampal pyramidal layer, related to Fig. 1C

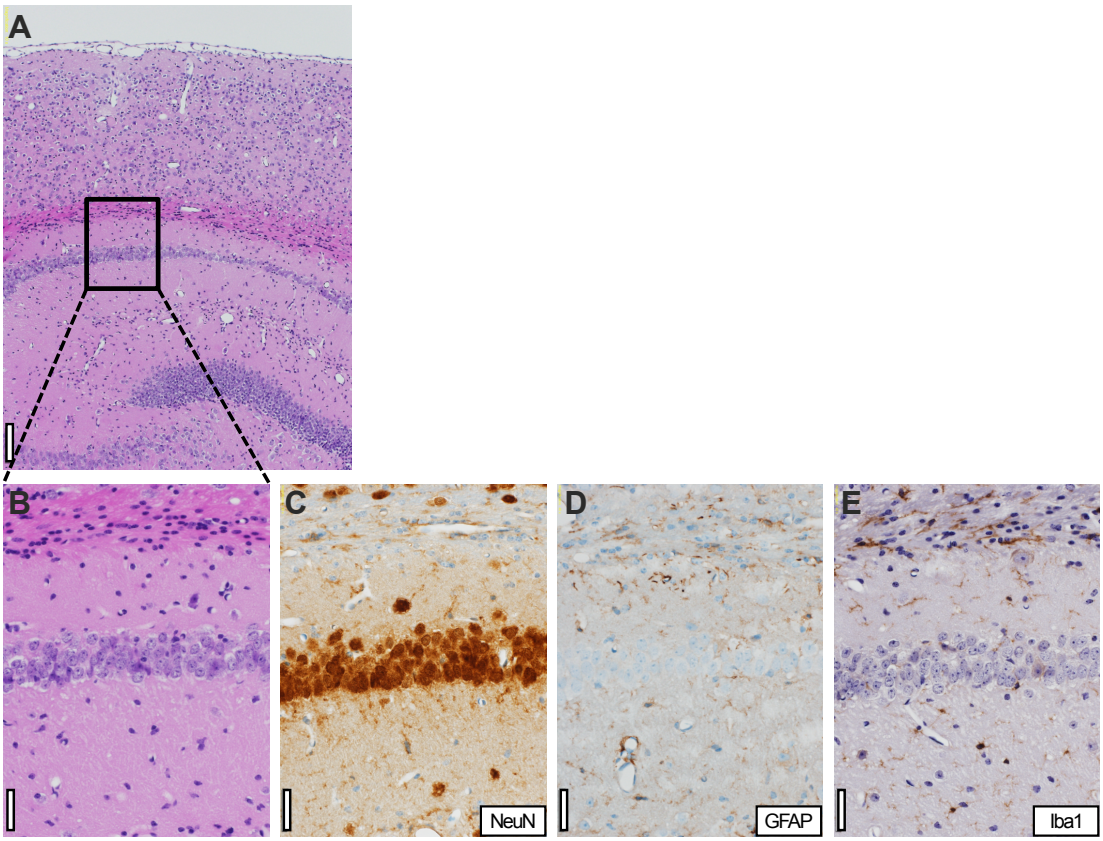

(A-E) Coronal cross-sections of hippocampal CA1 region stained with hematoxylin/eosin (A, B) or probed by immunohistochemistry for NeuN (C; neuronal), GFAP (D; astroglia), and Iba1 (E; microglia). Scale bars: 50μm (A), 20μm (B-E)

Fig. S2 Atf4 expression and target gene activation in Drp1-ablated brains, related to Fig. 1E-H

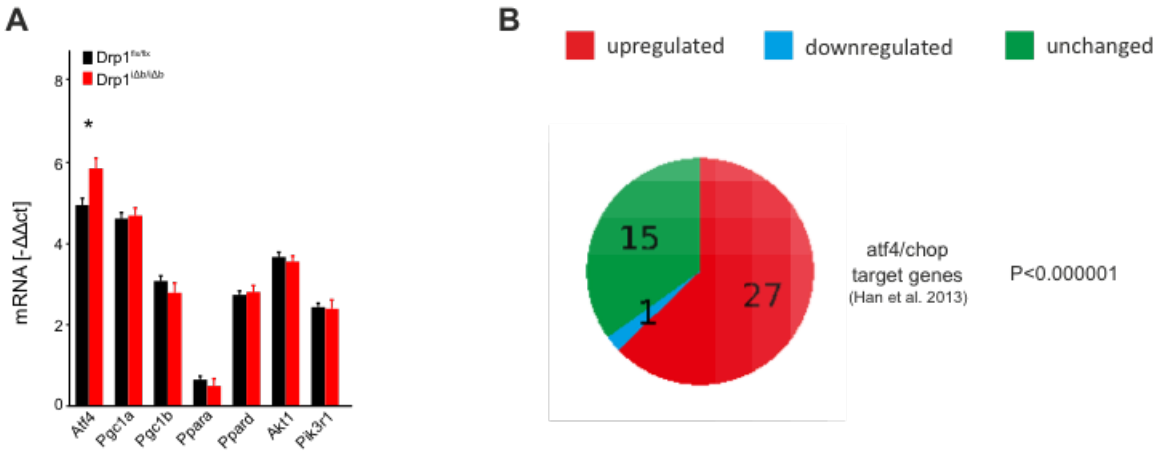

(A) mRNA expression in Drp1-ablated and control animals at 10 weeks PTI, normalized against 18S rRNA ct values. Data represent average ±SEM of at least 4 animals.

(B) Pie chart representing frequency distribution of up- and downregulated proteins of Drp1-ablated forebrain compared to wild-type brain.

Fig. S3 The mitochondrial UPR is not activated in Drp1-ablated brains, related to Fig. 3F-H

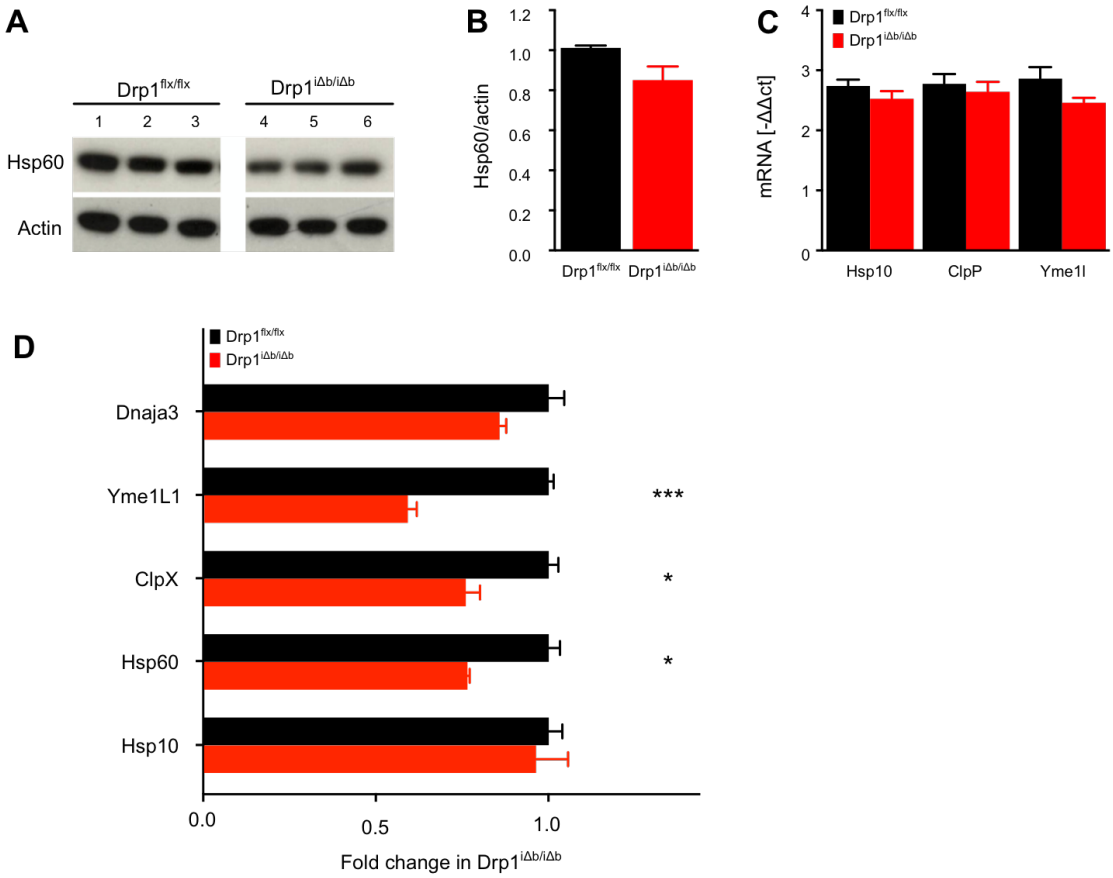

(A, B) Protein expression of mtUPR marker Hsp60 as determined by Western blot on hippocampal lysates at 10 weeks PTI, normalized to actin. Data represent average ±SEM of at least 4 animals.

(C) Hippocampal mRNA expression of *Hsp10*, *ClpP*, and *Yme1l* 10 weeks PTI as determined by qRT-PCR, normalized to 18S rRNA ct values. Data represent average ±SEM of at least 4 animals.

(D) Fold change in selected, mtUPR-related hits of a total proteomics screen 10 weeks PTI.

Asterisks in (D) denote q-values (i.e. p-values adjusted for multiple testing): *: $p<0.05$, ***: $p<0.001$.

SUPPLEMENTARY REFERENCES

Han, J., Back, S., Hur, J., Lin, Y., Gildersleeve, R., Shan, J., Yuan, C., Krokowski, D., Wang, S., Hatzoglou, M., et al. (2013). ER-stress-induced transcriptional regulation increases protein synthesis leading to cell death. Nat. Cell Biol. *15*, 481–490.

Moreno, J., Halliday, M., Molloy, C., Radford, H., Verity, N., Axten, J., Ortori, C., Willis, A., Fischer, P., Barrett, D., et al. (2013). Oral treatment targeting the unfolded protein response prevents neurodegeneration and clinical disease in prion-infected mice. Sci. Transl. Med. *5*, 206ra138.

Oettinghaus, B., Schulz, J., Restelli, L., Licci, M., Savoia, C., Schmidt, A., Schmitt, K., Grimm, A., Morè, L., Hench, J., et al. (2016). Synaptic dysfunction, memory deficits and hippocampal atrophy due to ablation of mitochondrial fission in adult forebrain neurons. Cell Death Differ. *23*, 18–28.

Ono, Y., Shimazawa, M., Ishisaka, M., Oyagi, A., Tsuruma, K., and Hara, H. (2012). Imipramine protects mouse hippocampus against tunicamycin-induced cell death. Eur. J. Pharmacol. *696*, 83–88.

Radford, H., Moreno, J., Verity, N., Halliday, M., and Mallucci, G. (2015). PERK inhibition prevents tau-mediated neurodegeneration in a mouse model of frontotemporal dementia. Acta Neuropathol. *130*, 633–642.